JOURNAL OF MATERIALS SCIENCE 25 (1990) 4087–4097

Failure mechanism in SMC subjected to alternating stresses

B. VON BERNSTORFF, G. W. EHRENSTEIN
Institute of Materials Technology, Kassel University, Wilhelmshöher Allee 73, D-3500 Kassel, West Germany

Failure mechanisms in randomly reinforced sheet moulding compounds subjected to fatigue testing were studied by relating the changes in characteristic mechanical properties to microscopic changes in the material. It was demonstrated that various mechanisms take place simultaneously to an extent that depends on the local microstructure and strength and that the collective interplay of these mechanisms is responsible for failure. As damage progresses, a uniform pattern of cracks is formed in the matrix, and Mode II fibre/matrix-interfacial failure occurs. The mechanisms concerned can be explained by calculating the forces transmitted between the fibres and the matrix. It was observed that different load amplitudes gave rise to equivalent damage patterns in the material. In the light of this fact and with the aid of the failure mechanisms identified, a method has been devised, by means of which the fatigue life can be estimated of SMC exposed to alternating loads of any given amplitude.

1. Introduction

By virtue of their costs and their beneficial mechanical properties, sheet moulding compounds (SMC) offer an attractive alternative to conventional materials [1]. This is evident in new fields of application, e.g. automobile parts that have to withstand both static and fatigue loads. Consequently, a deeper insight is required into the number of stress reversals that can be endured within a given time and the mechanisms involved in order to design SMC parts of adequate reliability and fatigue strength. The Wöhler method is usually adopted for determining the behaviour of a material exposed to stress cycles. The fatigue strength of metals and homogeneous polymers is governed by the propagation of a single crack. The critical state in which unstable crack propagation and failure occur can be uniquely described by the length of individual cracks and can also be predicted if the rate of crack propagation is known.

In contrast to this, different forms of damage occur alongside one another in heterogeneous materials, i.e. multi-phase composites. They depend on the local microstructure and strength, and the sum their contributions leads to failure of the material as a whole. The fatigue life of these materials can also be estimated if the failure mechanism related to the number of load cycles and a failure criterion that does not rely on the stress history are known. Consequently, the failure mechanism and the critical state at which failure occurs must be expressed in terms of mechanical properties by means of suitable test methods.

2. Fundamentals

In contrast to the formation of a single crack in homogeneous materials, various failure mechanisms occur in fibre-reinforced materials and they depend on the values for the elongation at break of the individual phases. A trivial case arises if the elongation at break of the matrix, ε_{Bm}, is equal to that of the fibres, ε_{Bf}, and failure is due to the formation of a single crack. For different elongations at break, i.e. $\varepsilon_{Bm} < \varepsilon_{Bf}$ and $\varepsilon_{Bm} > \varepsilon_{Bf}$, it depends on the volume fraction of fibres, V_f, whether one or more cracks is formed in either the matrix or the fibres. Suppose that the composite material consisting of two components is subjected to an axial tensile load. The properties of the two components are $V_1, E_1, \sigma_{B1}, \varepsilon_{B1}$ and $V_2, E_2, \sigma_{B2}, \varepsilon_{B2}$ respectively, and their cross-sections remain constant over the entire length (Fig. 1). At low values of strain in the range within which both components obey Hooke's law, the tensile stress applied to the composite is given by

$$\sigma = V_1 E_1 \varepsilon + V_2 E_2 \varepsilon \quad (1)$$

Now let the load increase until the strain in the more brittle phase is equal to the elongation at break. In this case, if $\varepsilon_{B1} > \varepsilon_{B2}$, the tensile strength of the composite is

$$\sigma_B = V_1 E_1 \varepsilon_{B2} + V_2 \sigma_{B2} \quad (2)$$

At the corresponding value of stress, the second phase fails, with the result that its share of the load must be borne by the first phase, which also fails if its tensile strength, σ_{B1} is not high enough or its volume fraction, V_1, in the composite is too small, i.e.

$$\sigma_{B1} V_1 < E_1 V_1 \varepsilon_{B2} + \sigma_{B2} V_2 \quad (3)$$

Hence, despite the difference in the values for the elongation at break, the entire composite fails owing to the formation of a single crack over the whole

0022–2461/90 $03.00 + .12

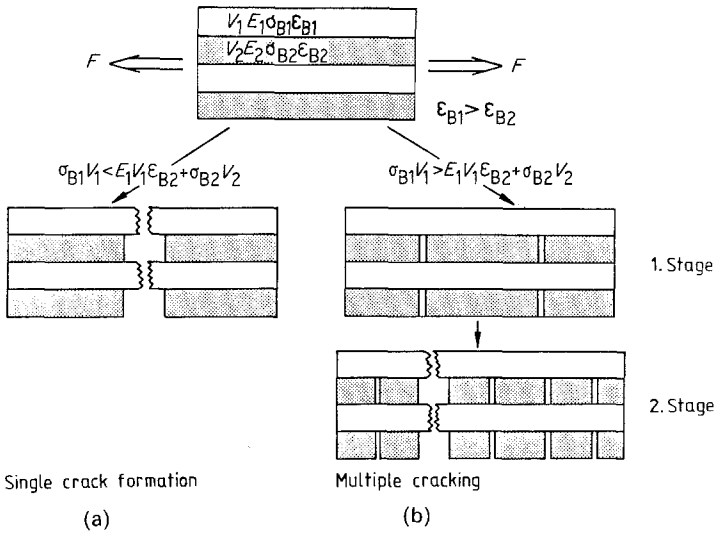

Figure 1 Possible fracture modes for composite materials with different ultimate strains of the components [2].

cross-section of the specimen (Fig. 1a). However, if the first phase had sufficient tensile strength, σ_{bl}, and its volume fraction, V_1, in the composite is large enough, it withstands the additional load transferred from the second phase, which has, in the meantime, failed. As the load on the composite increases, the more brittle phase progressively fragments, because the strong bond between the two phases prevents the complete stress relief that would otherwise result from crack formation. Hence, if the load is further increased up to a point corresponding to the higher elongation at break of the ductile phase, the low elongation at break of the brittle phase will be exceeded at several points in the composite. In this case, the failure mechanism proceeds in two stages: multiple crack formation in the brittle material (Stage 1) followed by fracture of the entire composite (Stage 2) caused by failure of the material with the higher elongation at break (Fig. 1b) [2].

Stress–strain curves and the relationship between the tensile stress at break for the composite and the volume fraction of fibres are shown in Fig. 2 for typical SMCs in which the elongation at break of the matrix is less than that of the fibres, i.e. $\varepsilon_{Bm} < \varepsilon_{Bf}$. The tensile stress at break for the composite, σ_B, can be expressed in terms of V_f by Equation 4

$$\sigma_B = \sigma'_f V_f + \sigma_{Bm} V_m \quad (4)$$

where $V_m = 1 - V_f$ is the volume fraction of the matrix and σ'_f is the stress in the fibres at the instant when the elongation at break of the matrix is reached.

At higher values of strain, the matrix fails as a result of multiple crack formation, and the strength of the composite is governed solely by the still intact structure of the fibres, i.e.

$$\sigma_B = \sigma_{Bf} V_f \quad (5)$$

Thus, as long as the matrix and the fibres share the load, the relationship between the tensile stress at break of the composite and the volume fraction of fibres will be the straight line represented by Equation 4. Afterwards, when the strength of the composite is governed solely by the fibres, because $\varepsilon_{Bm} < \varepsilon_{Bf}$, the relationship is given by Equation 5, i.e. the full line shown on the right in Fig. 2 [3].

As in the tensile case, multiple cracking occurs in fibre-reinforced composites that are subjected to alternating stresses. The spacing of cracks in 45° layer of laminate that had failed under tensile loading is compared in Fig. 3 to that in the corresponding layer stressed to failure in the fatigue test. The lower axis of abscissae represents the number of load cycles in the fatigue test; and the upper axis, the stress in the tensile test. The amplitude of the alternating stress was approximately $\hat{\sigma} = 400\text{N mm}^{-2}$, i.e. two-thirds of the tensile stress at break determined in the tensile test. Shortly before fracture occurred, the spacing between cracks was the same in both cases [4]. Obviously, a

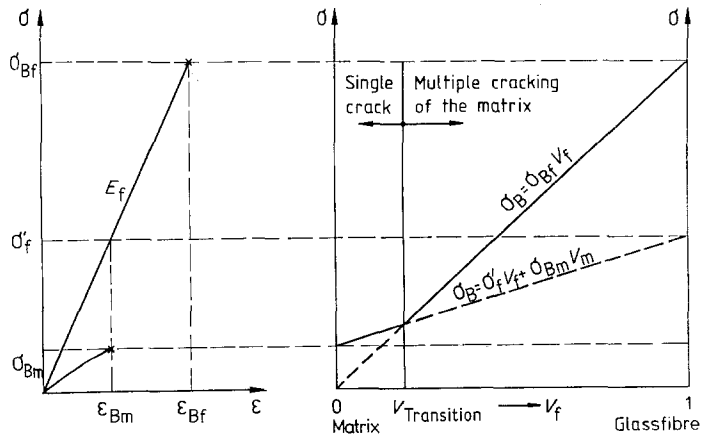

Figure 2 Single crack formation/multiple cracking transition as a function of glass fibre content.

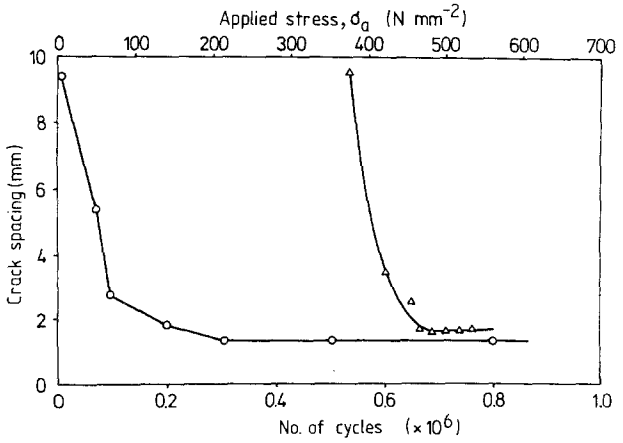

Figure 3 Crack plane distance in a 45° layer of a [0, 90 ± 45] laminate for (△) quasistatic and (○) fatigue loading [4].

maximum crack density exists for fibre-reinforced composites which is characteristic of the material but independent of the loading history. Because the crack density can be correlated directly with the stiffness of the specimen, Wurtinger and co-workers [5, 6] and later on Reifsnider *et al.* [7] proposed a stiffness-based fatigue failure criterion as the failure limit for composites subjected to alternating stresses.

The stiffness and residual strength have been plotted against the fatigue life in Fig. 4. The stiffness is reduced in three different stages, which allow the fatigue life to be divided into three ranges, each characterized by a different failure mechanism [8]. In the initial stage, which occurs early in the fatigue life, the stiffness drops rapidly owing to the formation of numerous transverse cracks in the matrix. A characteristic damage state (CDS), represented by a given pattern of cracks with uniform spacing [9], is reached after a few load cycles. A unique relationship between this characteristic damage state and the reduction in stiffness has been verified for numerous types of laminate [10].

In the second section of the curve shown in Fig. 4, delamination occurs along with cracking in the matrix [11] and the decrease in stiffness is merely slight. Towards the end of this section, the crack density is so high that no further cracks can be formed in the matrix. In fact, the matrix cracks coalesce, and there is a transition from multiple cracking to the formation of a single macroscopic crack.

The third section of the fatigue life curve is characterized by the propagation of this single crack and failure in the fibres associated with a pronounced decrease in strength and stiffness and failure of the specimen.

3. Materials investigated

The composition of the SMCs investigated was roughly as follows (the percentages represent mass fractions): 30% unsaturated polyester or vinylester resin (Palatal^R P 18 or Palatal^R V 7740, BASF AG, Ludwigshafen); 30% randomly oriented, glass fibre rovings of 25 mm length (Vetrotex P 233 textile glass rovings, Gevetex Textilglas GmbH, Herzogenrath) and 40% finely ground calcium carbonate (Millicarb^R, Omya GmbH, Cologne).

The resin also includes various additives such as Solpren 312 (Philips Petrolen Company) for shrinkage control, magnesium oxide for thickening, tertiary butyl perbenzoate as catalyst, zinc stearate as demoulding aid, and an impregnating agent. The lay-up of the laminates, together with local glass fibre and resin concentrations, is shown schematically in Fig. 5.

4. Dynamic properties of the materials

The aim of the study was to describe the complex fatigue mechanism in SMC by correlating various mechanical properties with the microstructural changes. For instance, the change in stiffness is a measure for the multiple crack formation during fatigue loading; and the mechanical damping, tan ϕ, for the degree of damage in the material. If the material displays linear viscoelastic behaviour, the angle, ϕ, is the phase shift between the exciting sinusoidal force and the value measured for the deformation. If the signals for the force and deformation are converted into stresses and strains, Equations 6 and 7 apply for the steady state,

$$\sigma(t) = \hat{\sigma} \sin \omega t \quad (6)$$

$$\varepsilon(t) = \hat{\varepsilon} \sin (\omega t - \phi) \quad (7)$$

where $\hat{\sigma}$ and $\hat{\varepsilon}$ are the stress and strain amplitudes.

If the sinusoidal stress and strain signals are superimposed to eliminate time, an elliptical σ–ε

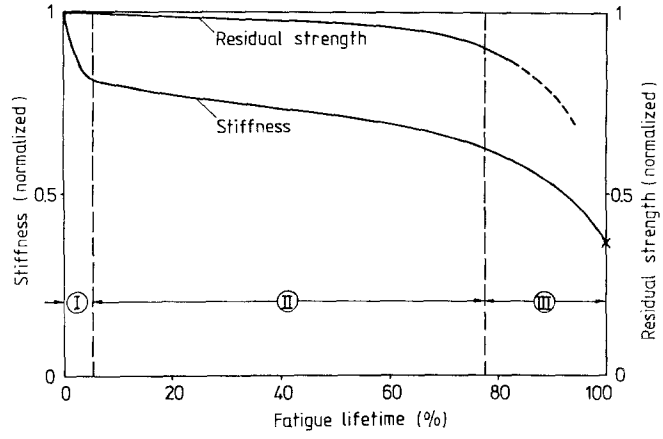

Figure 4 Stiffness reduction and residual strength for fatigued composites [8].

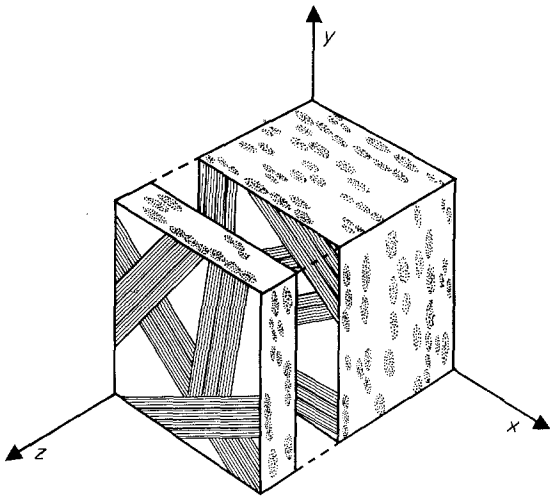

Figure 5 Schematic structure of SMC.

hysteresis loop is obtained

$$\sigma(t) = \varepsilon(t)\frac{\hat{\sigma}}{\hat{\varepsilon}}\cos\phi + \hat{\sigma}\sin\phi\left\{1 - \left[\frac{\varepsilon(t)}{\hat{\varepsilon}}\right]^2\right\}^{1/2} \quad (8)$$

If the relationship

$$\hat{\sigma}\sin\phi\left\{1 - \left[\frac{\varepsilon(t)}{\hat{\varepsilon}}\right]^2\right\}^{1/2} \geqslant 0 \text{ for } A \leqslant \varepsilon(t) \leqslant C$$
$$\leqslant 0 \text{ for } C \leqslant \varepsilon(t) \leqslant A \quad (9)$$

is positive for $\varepsilon(t) = \hat{\varepsilon}\sin(\omega t - \phi)$, the sum of the two terms in Equation 8 gives rise to the upper section $\overset{\frown}{ABC}$ of the stress–strain hysteresis loop. Likewise, if the expression is negative, the lower section $\overset{\frown}{CDA}$ will be obtained (Fig. 6). Therefore, the same amounts with respect to $\varepsilon(t)$ are added or subtracted. Hence, the straight line represented by the first term of Equation 8 halves the stress–strain hysteresis loop and is referred to as the centre curve in the hysteresis loop whose slope is a measure of the material's stiffness.

Imagine that mechanical damping in a linear viscoelastic material is gradually reduced to zero. In this case, the stress–strain hysteresis loop will progressively become more slender until, finally, the upper and lower sections coincide with the curve in the centre. The centre $\overset{\frown}{AC}$ is obtained as the stress–strain curve for a linear elastic material in the limiting case of Equation 8, i.e.

$$\lim_{\phi\to 0}\sigma(t) = \varepsilon(t)\frac{\hat{\sigma}}{\hat{\varepsilon}} \quad (10)$$

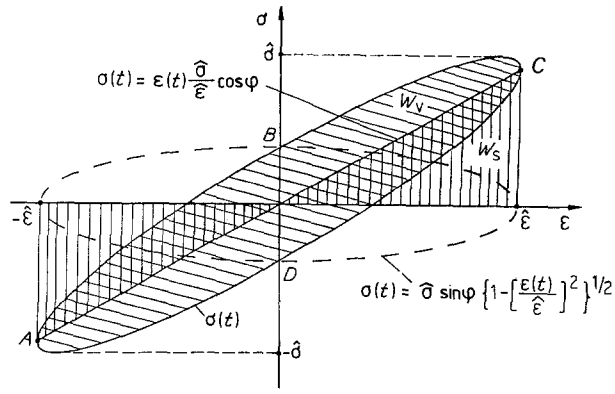

Figure 6 Stress–strain hysteresis loop for linearly viscoelastic material.

Hence, the vertically hatched area under the centre curve in Fig. 6 is a measure of the energy, W_S, stored in an element of volume while the material is being subjected to alternating stresses, i.e.

$$W_S = \int_{-\hat{\varepsilon}}^{+\hat{\varepsilon}}\sigma(\varepsilon)\,d\varepsilon = \frac{\hat{\sigma}}{\hat{\varepsilon}}\cos\phi\int_{-\hat{\varepsilon}}^{+\hat{\varepsilon}}d\varepsilon = \hat{\sigma}\hat{\varepsilon}\cos\phi \quad (11)$$

The energy per unit volume dissipated during a complete load cycle, i.e. the loss energy, W_L, is obtained by integrating the area enclosed by the hysteresis loop, i.e.

$$W_L = \oint\sigma(\varepsilon)\,d\varepsilon = \pi\hat{\sigma}\hat{\varepsilon}\sin\phi \quad (12)$$

Then, the mechanical damping can be obtained by expressing the loss energy, W_L, as a ration of the storage energy, W_S, i.e.

$$W_L/W_S = \frac{\pi\hat{\sigma}\hat{\varepsilon}\sin\phi}{\hat{\sigma}\hat{\varepsilon}\cos\phi} = \pi\tan\phi \quad (13)$$

The dynamic characteristics for nonlinear viscoelastic materials can also be derived from the nonelliptical hysteresis loop by formally defining a centre curve that halves the loop for each value of strain. In this case, the area under the centre curve again corresponds to the storage energy, W_S; and that enclosed by the hysteresis loop represents the loss energy, W_L. The ratio W_L/W_S is again an expression for the mechanical damping.

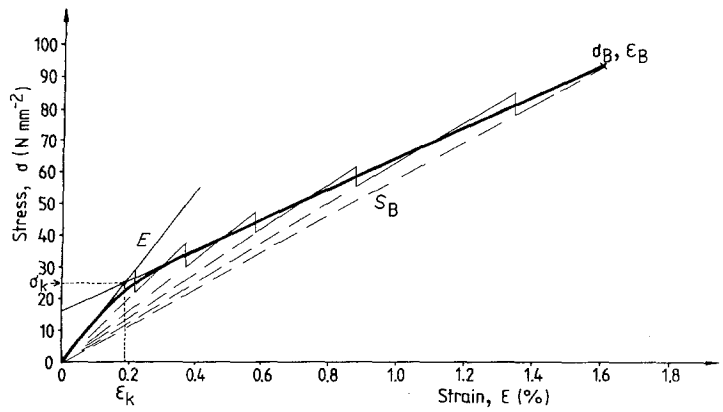

Figure 7 Stress–strain diagram of SMC and geometrical evaluation of the knee point. S_B = specimen stiffness at break. $\sigma_k = 25.30\,N\,mm^{-2}$, $\varepsilon_k = 0.19\%$, $\sigma_B = 94.02\,N\,mm^{-2}$, $\varepsilon_B = 1.61\%$, $E = 13\,180\,N\,mm^{-2}$, $S_B = 5870\,N\,mm^{-2}$.

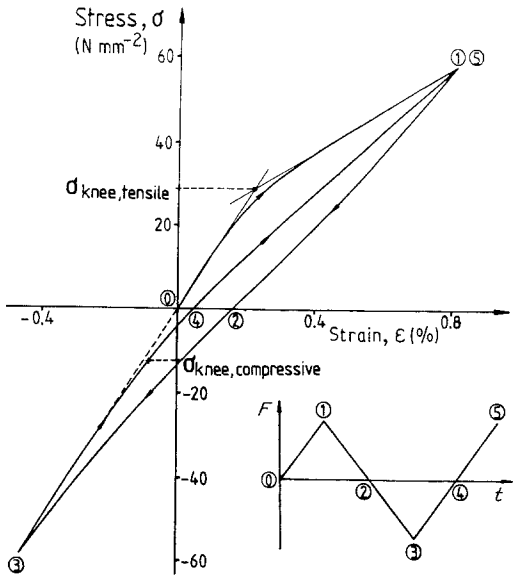

Figure 8 First stress–strain hysteresis loop.

5. Experimental details

5.1. Tensile test

In the stress–strain diagram obtained in the tensile test on SMC, a pronounced knee occurs at 0.2% to 0.3% strain. Above this knee point, the curve is flat and almost linear, and the first signs of multiple cracking in the matrix become evident. The number of cracks then increases up to the point where the specimen fails (Fig. 7).

In Fig. 7, steps have been formed in the flatter branch of the stress–strain curve above the knee point. These are intended to convey that the curve consists of numerous small stress jumps. It is assumed that cracks in the matrix of SMC are interrupted at the interfaces with the bundles of glass fibre rovings. If the fibre bundles are firmly bonded to the matrix and the crack has to be propagated beyond the obstacle that they present, they must stretch until an elongation is reached that is large enough to permit further matrix crack propagation. Because the matrix and the fibres have different elongations at break and moduli of elasticity, much energy is required to effect these elongations. Consequently, the fibres present an effective barrier to the propagation of individual cracks and

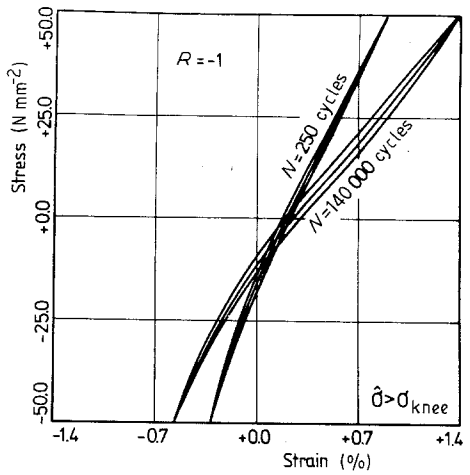

Figure 9 Stress–strain hysteresis loops for $\hat{\sigma} > \sigma_{knee}$.

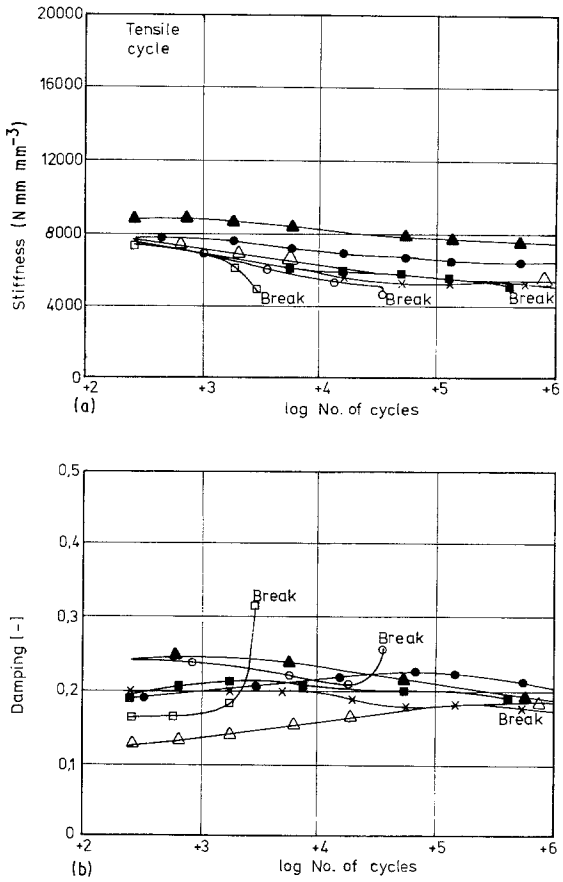

Figure 10 (a) Stiffness and (b) damping for various stress amplitudes as a function of number of cycles. Stress amplitudes ($\hat{\sigma}$, N mm^{-2}):(▲) ±20, (●) ±25, (■) ±30, (x) ±35, (△) ±40, (○) ±50, (□) ±60.

thus allow greater opportunity for the formation of new cracks, i.e. multiple crack formation, in the matrix. Hence, as the strain increases, the specimen becomes less rigid up to the instant of failure (cf. the curves for the secant moduli shown by dotted lines in Fig. 7).

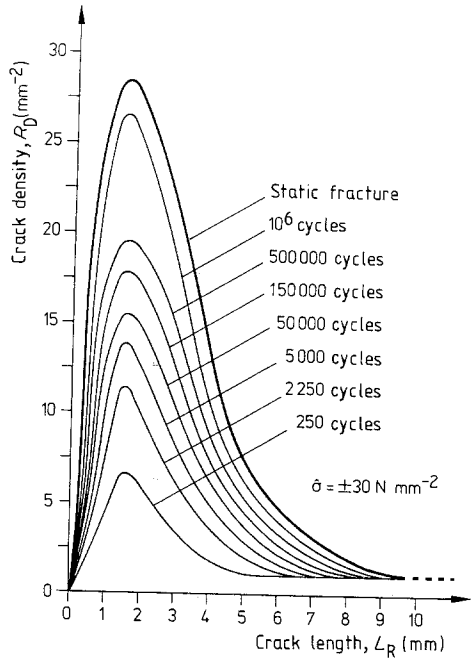

Figure 11 Crack length distributions as a function of fatigue time. For comparison, the crack length distribution of a quasistatic fractured specimen is also plotted.

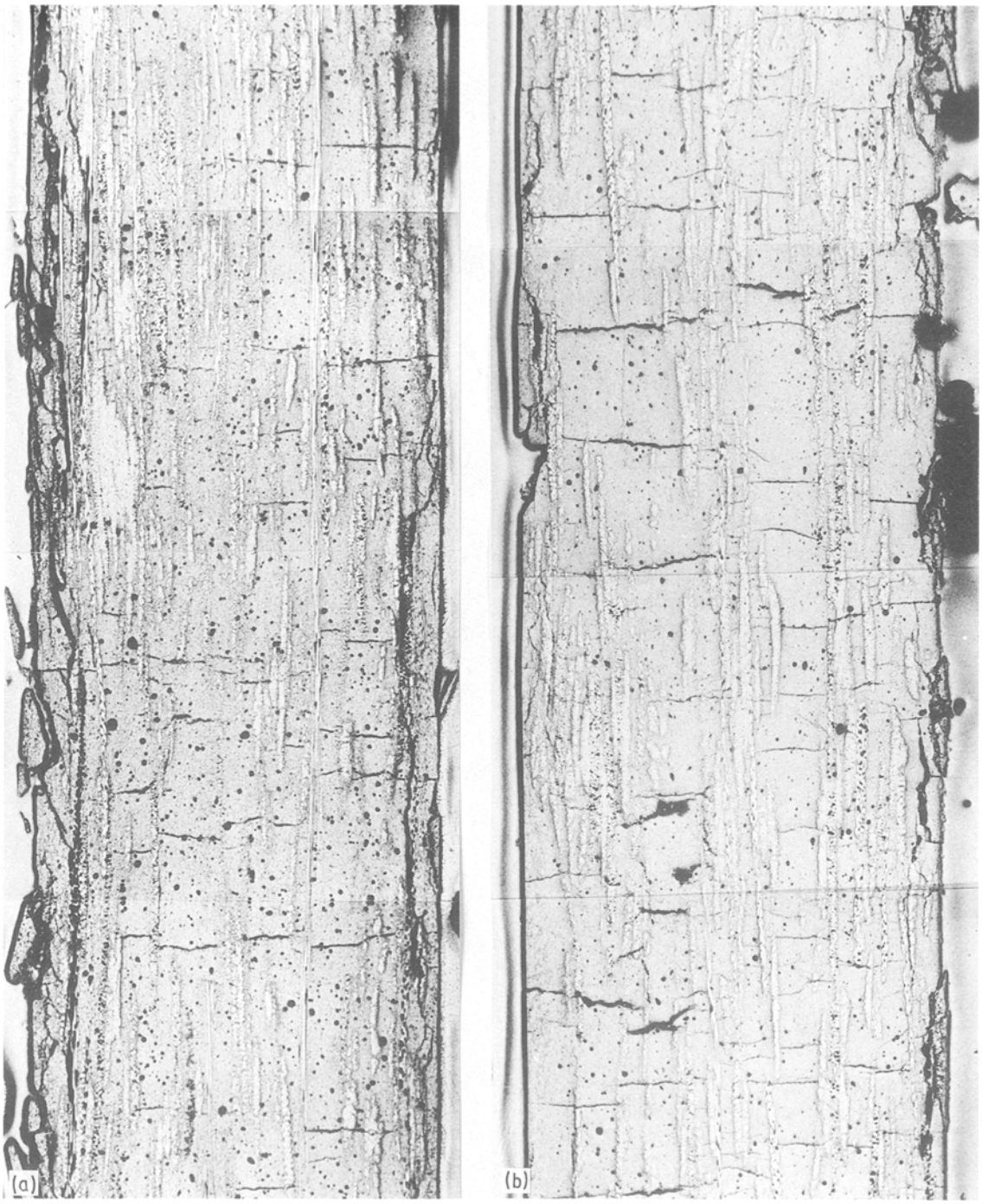

Figure 12 Multiple cracking of the matrix after N = (a) 1000 cycles and (b) 5000 cycles for $\hat{\sigma} = 30\,\mathrm{N\,mm^{-2}}$. Microsection of the y–z plane.

5.2. Tensile and compressive stress

The first complete cycle in the fatigue test was studied in detail by reducing the rate of straining SMC during tension and compression on a tensile tester.

If $\sigma_{max} \leqslant \sigma_{knee}$, the stress–strain curves for the material in tension and compression are symmetrical about the origin. However, their shapes differ considerably if $\sigma_{max} < \sigma_{knee}$, as demonstrated in Fig. 8. First of all, a tensile stress roughly equal to 80% of the tensile strength is applied to the specimen. As a result of the microcracks formed in the matrix, the stiffness is reduced, and the knee can thus be seen in the stress–strain diagram. At about $\sigma = 0.8\sigma_B$, the load is removed from the specimen (Position 1). The residual strain (Position 2) remains until it is cancelled by the subsequent compressive load. As the compressive stress increases until the strain is in the range $\varepsilon \leqslant 0$, the matrix becomes more rigid again, with the result that an initially hardly discernable discontinuity occurs in the stress–strain diagram. At a compressive stress of $\sigma = -0.8\sigma_B$ (Position 3), the load on the specimen is again relieved. The stress–strain curve then runs in the direction of the origin, but its slope decreases at $\varepsilon \leqslant 0$. Hence, in the unstressed state after the first complete load cycle (Position 4), the specimen is elongated, and the hysteresis loop remains unclosed until the tensile load in the next cycle is applied (Position 5). In this case, there is no knee in the curve for the repeated tensile cycle.

Thus, in the first complete tension/compression cycle, three changes that significantly affect fatigue occur in the hysteresis loop: the shift from the origin

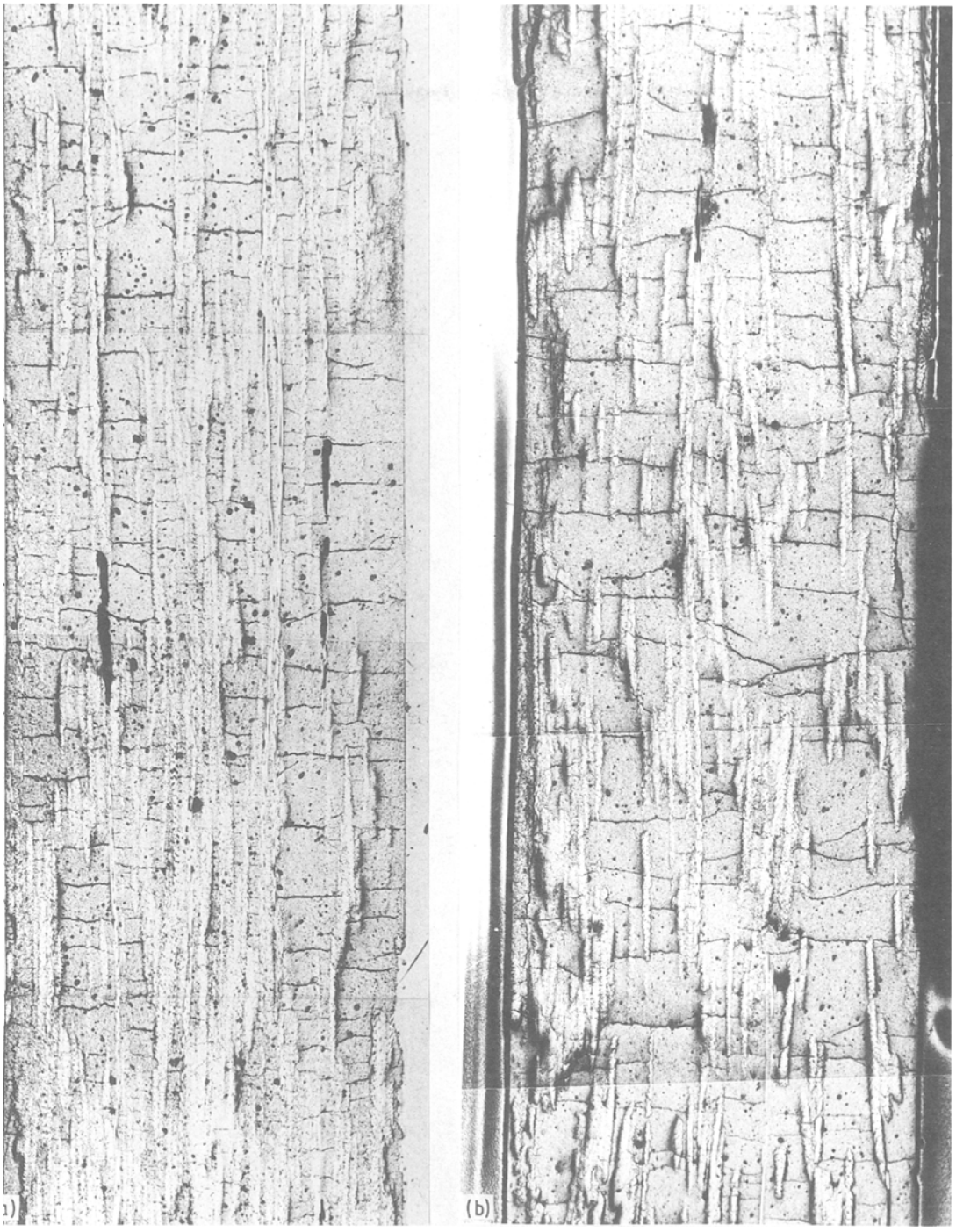

Figure 13 Final crack pattern of a fatigued ((a) $\hat{\sigma} = 30\,\mathrm{N\,mm^{-2}}$) and (b) a quasistatic fractured specimen. Microsection of the y–z plane.

in the direction of positive values of strain, the occurrence of a discontinuity in the compression section, and the absence of the knee in the tension section.

5.3. Fatigue test

The first and last hysteresis loops determined before failure under an alternating of $\hat{\sigma} = \pm 50\,\mathrm{N\,mm^{-2}}$ are shown in Fig. 9. After $N = 250$ load cycles, the hysteresis loop shifts from the origin in the direction of positive strains, and the discontinuity in compression is observed at $\varepsilon = 0$. The differences in tensile and compressive stiffness increase up to the point of failure and accentuate the discontinuity.

Fig. 10 shows the stiffness reduction and mechanical damping of SMC for various stress amplitudes as functions of the number of loads cycles. In anticipation of the results of fractographic analysis, it can be said that the steady decrease in stiffness within a tension cycle can be ascribed to a continuous increase in the crack density. A striking fact is that the specimen does not fail until the ultimate stiffness falls below the value measured in the tensile test.

The damping curves start to rise at low values of stress amplitude. They pass through a maximum at an amplitude slightly higher than the static tensile knee stress $\hat{\sigma} \geqslant \sigma_{\mathrm{knee}}$, and decrease again for higher amplitudes. In the initial stages, the loss energy per cycle outweighs the storage energy and the damping increases. Afterwards, owing to the low slope of the hysteresis curve, the storage energy increases more than the loss energy and causes a decrease of the damping.

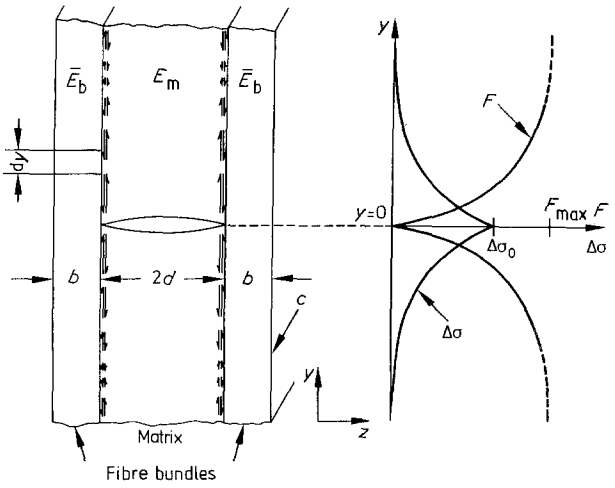

Figure 14 Force transformation by shear stresses in the matrix/fibre bundles interface.

5.4. Fractographic studies

Multiple cracks were formed on the surface of all the SMC specimens that were subjected to alternating stresses. The cracks were counted and measured, and their length distribution was plotted against the number of load cycles. The crack length distribution of a specimen that had failed in the tensile test was included in the diagram (Fig. 11). No change occurs in the shape of the distribution curves but the number of cracks increases and therefore, the endurance of SMC is largely governed by the formation of new cracks and not by the propagation of a few cracks. Furthermore, a comparison of the length distributions for specimens that had failed under static and dynamic loads gives rise to the assumption that alternating stresses increase the number of cracks to that of statically fractured specimens.

The following diagrams show y–z sections through an unsaturated polyester SMC subjected to alternating stresses, i.e. after $N = 1000$ and 5000 load cycles (Fig. 12) and after fatigue failure (Fig. 13a). A section through a specimen that had failed in the tensile test is shown as a comparison (Fig. 13). Wherever the thickness of the matrix between the layers of fibres remains constant over large areas, the crack spacing is uniform. Thick layers of matrix give rise to large crack spacings; and, conversely, thin layers of matrix, to very close crack spacing.

A comparison of the diagrams reveals a feature of fatigue failure: the number of cracks in the matrix increases and the uniform spacing between the cracks becomes closer to the same extent as that of a specimen that has failed in the static tensile test.

6. Failure mechanisms

It was demonstrated in Fig. 1 that, if the elongation at break of the fibres was different from that of the matrix and if the volume fractions of the two phases were given, redistribution of forces would give rise to multiple cracking. Because the redistribution is caused by the transmission of shear stresses in the matrix/fibre interface, the shear strength of the interface evidently governs the spacing between the cracks in the matrix [12].

If an external load is applied, the difference between the stiffness of the matrix and that of the layer of fibre bundles gives rise to shear stresses in the interface (Fig. 14). In each increment of interface dy, these shear stresses transmit a force dF from the layer of fibre bundles into the matrix, where dF is given by

$$dF = 2c\tau\, dy \tag{14}$$

Cracks occur in the matrix if the force F

$$F = 2\sigma_{Bm} dc \tag{15}$$

is exceeded.

As a result of the cracks in the matrix, the component of load supported by an element of area in the matrix must now be borne in the form of an additional stress, $\Delta\sigma$, by the layer of fibre bundles. In the plane of the cracks, this additional stress attains a maximum, $\Delta\sigma_0$, given by

$$\Delta\sigma_0 = \frac{\sigma}{V_b} - \frac{\sigma\bar{E}_b}{E_{SMC}} \tag{16}$$

where σ is the externally applied stress, $\bar{E}_b$ is the transverse isotropic modulus of elasticity for the layer of fibre bundles, and E_{SMC} is the modulus of elasticity for the entire SMC composite.

As the distance y from the plane of the crack increases, the additional stress, $\Delta\sigma$, decreases in proportion to the extent to which it is retransmitted by the interfacial shear stresses from the layer of fibre bundles into the matrix (Fig. 14). According to a modified shear lag theory for elastic coupling between the matrix and the bundle of fibres, Equation 17 applies for the additional stress

$$\Delta\sigma = \Delta\sigma_0 \exp(-\Phi^{1/2} y) \tag{17}$$

where the constant Φ is given by [13]

$$\Phi = \frac{E_{SMC} G_m}{\bar{E}_b E_m}\left(\frac{b + d}{bd^2}\right) \tag{18}$$

The shear stress in the interface is derived from the equilibrium of forces acting on an element of volume in the layer of fibres, i.e.

$$\tau c\, dy = \Delta\sigma bc - (\Delta\sigma + d\Delta\sigma)bc$$

or

$$\tau = -b\frac{d\Delta\sigma}{dy} \tag{19}$$

Differentiating Equation 17 and inserting Equation 19 gives the relationship for the shear stress, i.e.

$$\tau = b\Delta\sigma_0\Phi^{1/2} \exp(-\Phi^{1/2} y) \tag{20}$$

Inserting this expression for the shear stress in Equation 14 then gives the force

$$dF = 2cb\Delta\sigma_0\Phi^{1/2} \exp(-\Phi^{1/2} y)\, dy$$

transmitted per increment of interface.

By integrating, the force retransmitted into the matrix is obtained as a function of the distance, y, from the plane of the cracks

$$F = 2cb\Delta\sigma[1 - \exp(-\Phi^{1/2} y)] \tag{21}$$

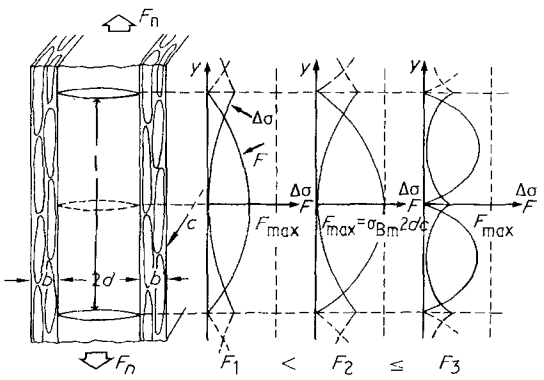

Figure 15 Multiple crack formation in the matrix layer under increasing tensile force.

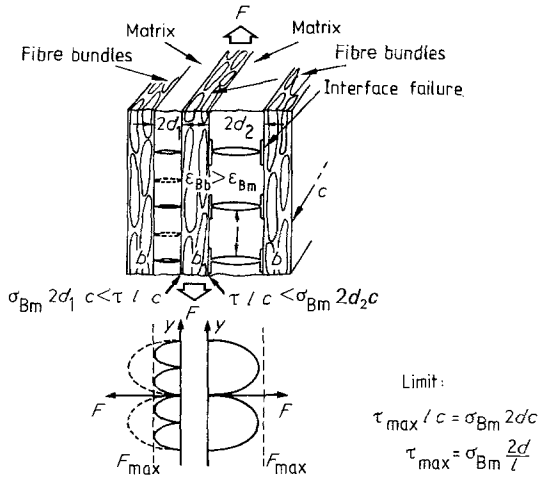

Figure 16 Interfacial failure in the thick and multiple cracking in the thin matrix layer for increasing tensile forces.

The curve for the force retransmitted into the matrix is shown in Fig. 14. Because the load in the matrix increases with the distance from the plane of cracking, further cracks are formed mid-way between those already existing when the force in the matrix exceeds $2\sigma_{Bm}dc$, and hence with Equation 21.

$$2\sigma_{Bm}dc = 2cb\Delta\sigma_0[1 - \exp(-\Phi^{1/2}y)] \quad (22)$$

According to Equation 16, the additional stress, $\Delta\sigma_0$, in the fibre bundles increases with the externally applied tensile stress, σ. Thus the number of cracks formed between those already existing in the matrix continues to grow, with the result that, according to Equation 22, the spacing $y = l$ in the pattern of equidistant cracks becomes continuously closer (Fig. 15):

$$l = -\frac{1}{\Phi^{1/2}} \ln\left(1 - \frac{\sigma_{Bm}d}{\Delta\sigma_0 b}\right) \quad (23)$$

As the externally applied load increases, the forces that are caused by shear stresses and are transmitted by the matrix/fibre bundle interface become progressively larger. If the shear stresses exceed the interfacial shear strength before the retransmitted forces become large enough to overcome the tensile strength of the matrix and thus to initiate new cracks, the interface will fail by delamination of the fibre bundles from the matrix [14, 15]. According to Equation 20, the maximum interfacial shear strength, i.e. the origin of delamination, occurs at $y = 0$ in the plane of crack formation and is given by

$$\tau_{max} = b\Delta\sigma_0\Phi^{1/2} \quad (24)$$

As opposed to this, the forces retransmitted from the fibres into the matrix attain a maximum at $y = \pm l/2$ (cf. Fig. 15). The interfacial shear strength then follows from the equilibrium of forces according to Equations 14 and 15, i.e.

$$\tau_{max} = \sigma_{Bm}\frac{2d}{l} \quad (25)$$

Accordingly, the ratio $2d/l$ of the matrix thickness to the crack plane spacing is constant throughout the entire material. This can be easily verified in Figs 12 and 13. It can also be seen from Fig. 13 that the spacing between the crack planes is larger in thick than in thin layers of the matrix. However, if the strength of the matrix is the same but the cross-sectional area is less, the forces that can be endured are correspondingly less. Because the forces retransmitted by shear forces into the matrix are independent of the matrix thickness, they exceed the strength of the matrix in thinner layers

$$\tau lc > \sigma_{Bm}2dc$$

and thus initiate further cracking. However, the maximum forces that can be endured in thicker layers of matrix remain greater than the forces retransmitted along the interfaces

$$\tau lc < \sigma_{Bm}2dc$$

and interfacial failure occurs (Fig. 16).

Obviously, different failure mechanisms occur simultaneously if quasistatic stresses are applied. They differ according to the thickness of the layer of matrix: in thick layers, the ultimate crack spacing is first reached, and subsequently applied tensile stresses then delaminate the fibre bundles from the matrix. In thin layers of matrix, the crack spacing becomes increasingly less until a minimum is reached at $2d/l = \tau/\sigma_{Bm}$ and interfacial failure occurs.

The fact that different failure mechanisms proceed simultaneously provides the key to clarifying the progressive formation of multiple cracks in the fatigue test with loads of constant amplitude. The ratio $2d/l$ between the thickness of the matrix layer and the crack plane spacing was measured from a broken specimen. Fig. 12 shows that even for a short-time fatigued specimen the minimum possible spacing between the crack planes was already reached in a few thick layers of the matrix. On further application of fatigue loads, interfacial failure due to matrix/fibre delamination originating from the crack planes occurs in these matrix layers. Owing to the difference between the stiffness of the fibre bundles and that of the layers of the matrix in SMC, Mode II alternating shear stresses delaminate the matrix from the fibres to an extent depending on the number of load cycles.

The more this delamination progresses along the layers of fibres, the less is the share of the force transmitted by the fibres (Fig. 17b) and the greater the stresses in the remaining cross-section (Fig. 17a). As a

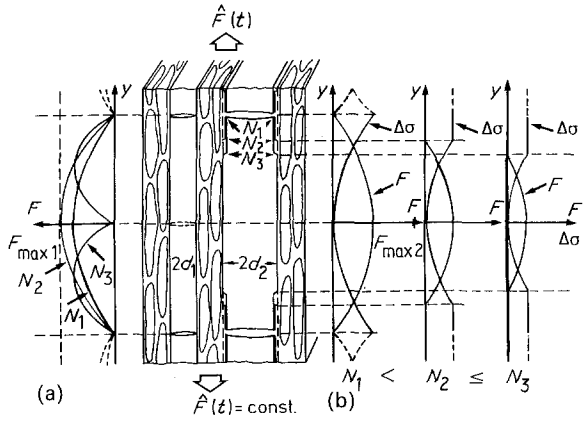

Figure 17 Progressive matrix/fibre bundle delamination in the thick matrix layer causes increasing stresses and multiple cracking in the thin matrix layer depending on the number of load cycles for fatigue loading.

result, multiple cracks are formed in the narrower layers of the matrix. The progressive interfacial failure is responsible for a continuous increase in the stresses acting in the remaining cross-sections and leads to further crack formation in the matrix with a decrease in the spacing between the crack planes. Finally, the minimum spacing will also be reached in the narrower layers of the matrix, with the result that these will also undergo interfacial failure.

Thus the failure caused by continued fatigue loading traverses the entire specimen. It assumes the form of multiple cracks that are first formed in the thicker layers of the matrix and are then displaced into progressively narrower layers.

7. Conclusions

The failure mechanisms that occur in cyclic loading are the formation of multiple cracks in the matrix, interfacial failure, and progressive delamination of the fibre bundles from the matrix. The only one among them that is a fatigue mechanism is progressive delamination, in which the delamination front is lengthened in increments during each cycle of Mode II alternating stress. Although different failure mechanisms can be assigned to progressive delamination under quasistatic and alternating stresses, that responsible for fatigue is the formation of multiple cracks. The reason for this is evident from the structure of the SMC: in view of the great differences in thickness of the matrix layers, interfacial failure followed by progressive delamination always occurs only in those layers that have already become saturated with multiple cracks. As the fatigue load is prolonged, the layers of matrix that are traversed by multiple cracks become narrower and narrower until the equidistant crack spacing in them becomes a minimum, i.e. the crack density reaches its maximum. It is not until this point is reached that interfacial failure with progressive delamination can set in. This consecutive mechanism was derived from the case of quasistatic stress and is responsible for the fact that a constant layer-thickness/crack-spacing ratio of $2d/l$ also applies to SMC specimens subjected to alternating stresses. Consequently, the effects of the failure mechanisms on the pattern of cracks and thus the stiffness of the specimen at failure are the same in both cases (cf. Fig. 13).

Owing to this equivalent relationship between the stress and the number of load cycles, neither the stiffness nor the pattern of cracks allows a conclusion on whether damage in SMC specimens has been caused by quasistatic or alternating stress. A similar equivalence exists between the stress amplitude and the number of load cycles in fatigue tests in which the stress amplitude is varied. As a result, the same state of damage as that reached after very long endurance periods can be achieved by superimposing a number of shorter fatigue tests in which the stress amplitude is progressively increased. Because the stiffness steadily decreases during the fatigue test, the individual stiffness/stress amplitude curves (cf. Fig. 10) can be shifted and arranged in sequence with respect to the reference amplitude along the axis for the number of load cycles. By this means, a master curve can be drawn for the stiffness of a specimen subjected to alternating stresses up to failure (Fig. 18). A master curve compiled in a similar manner for the mechanical damping has been included in the diagram.

Another conclusion that can be drawn from the equivalent relationship between the stress and the number of load cycles is that the secant modulus passing through the point of failure in the tensile stress–strain diagram is a suitable stiffness failure criterion for SMC specimens subjected to alternating stresses. In Fig. 19, an example is shown of a master curve in which the limiting stiffness for the secant modulus criterion has been included.

The three fatigue phases can be readily followed over the entire length of the curves for the stiffness and mechanical damping. The first phase consists of the incipient formation of multiple cracks up to the characteristic damage state (CDS), which is characterized by a pronounced decrease in stiffness and in the corresponding damping maximum. In the second phase, the stress in the specimen gradually increases

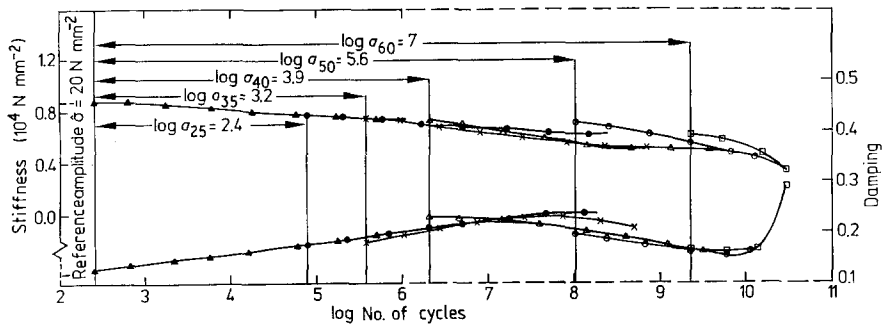

Figure 18 Construction of stiffness and damping master curves for fatigued SMC. Data taken from Fig. 10.

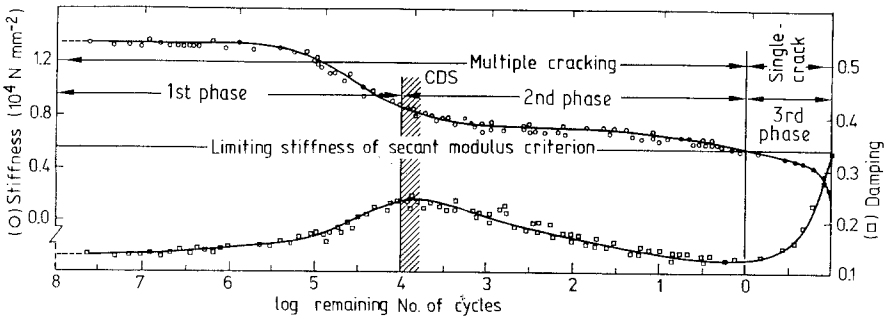

Figure 19 Three stages of fatigue failure and life time estimation according to the secant modulus failure criterion.

owing to progressive delamination and the ensuing continuation of multiple crack formation, which is associated with a further decrease in stiffness. In the third fatigue phase, a transition takes place from the formation of multiple cracks to the formation of a single propagating crack. It results in a further, pronounced decrease in stiffness and a large increase in damping.

The point at which the third phase commences in Fig. 19 was fixed, somewhat arbitrarily at first, by the limiting stiffness for the secant modulus criterion. The reason for this was that the transition from multiple to single crack propagation cannot be determined precisely from the stiffness curve itself. It was not until the master curves for stiffness and damping were constructed that it was noticed that the limiting stiffness for the secant modulus criterion coincided with a local damping minimum. This is due to the superimposition of two opposing mechanisms, i.e. decreased damping in the repeat cycles and increased damping by single crack propagation. It thus indicates the transition to the propagation of a single crack.

If the number of load cycles in the stiffness curve for SMC specimens subjected to various stress amplitudes is counted backwards, starting from the limiting stiffness, the number of load cycles remaining allows an estimate of the fatigue life to be made. For this purpose, the stiffness remaining after the first tensile stress cycle is determined for a given stress amplitude in the tensile test illustrated in Fig. 7. The number of load cycles corresponding to this figure on the stiffness curve represents the number remaining up to failure.

References

1. R. RENZ, V. ALTSTÄDT and G. W. EHRENSTEIN, *Reinf. Plastics Composites* **7** (1988) 413.
2. G. A. COOPER, "Fracture and Fatigue", Vol. 5 (Academic Press, New York, London, 1974).
3. K. FRIEDRICH, "Fortschrittsberichte der VDI-Zeitschriften", Vol. 18 (VDI-Verlag, Düsseldorf, 1984).
4. K. L. REIFSNIDER, K. SCHULTE and J. C. DUKE, "Long Term Behavior of Composites", ASTM STP 813 (American Society for Testing and Materials, Philadelphia, Pennsylvania, 1983).
5. K. H. HELLWEGE and H. WURTINGER, *Z. Kunststoffe* **48** (1968) 163.
6. W. KNAPPE and H. WURTINGER, *ibid.* **59** (1969) 975.
7. K. L. REIFSNIDER, W. W. STINCHCOMB and T. K. O'BRIEN, "Fatigue of Filamentary Composite Materials", ASTM STP 636 (American Society for Testing and Materials, Philadelphia, Pennsylvania, 1977).
8. K. SCHULTE, K. L. REIFSNIDER and W. W. STINCHCOMB, **18** (AVK-Jahrestagung, Freudenstadt, 5-8 October, 1982).
9. A. L. HIGHSMITH and K. L. REIFSNIDER, in "Damage in Composite Materials", ASTM STP 775 (American Society for Testing and Materials, Philadelphia, Pensylvania, 1982).
10. T. K. O'BRIEN and K. L. REIFSNIDER, *J Test. Eval.* **5** (1977) 384–393.
11. T. K. O'BRIEN, in "Damage in Composite Materials", ASTM STP 775 (American Society for Testing and Materials, Philadelphia, Pennsylvania, 1982).
12. J. AVESTON and A. KELLY, *J. Mater. Sci.* **8** (1973) 352–362.
13. K. W. GARRETT and J. E. BAILEY, *ibid.* **12** (1977) 157–168.
14. J. E. BAILEY and A. PARVIZI, *ibid.* **16** (1981) 649–659.
15. G. W. EHRENSTEIN and R. WURMB, *Angew. Makromol. Chemie* **60/61** no. 851 (1977) 157–214.

Received 24 April
and accepted 29 September 1989